Chemico-Biological Interactions 374 (2023) 110380

Contents lists available at ScienceDirect

Chemico-Biological Interactions

journal homepage: www.elsevier.com/locate/chembioint

Research paper

Investigating the competition between ACE2 natural molecular interactors and SARS-CoV-2 candidate inhibitors

Edoardo Milanetti [a,b,*], Mattia Miotto [b], Leonardo Bo' [b], Lorenzo Di Rienzo [b], Giancarlo Ruocco [a,b]

[a] Department of Physics, Sapienza University, Piazzale Aldo Moro 5, 00185, Rome, Italy
[b] Center for Life Nanoscience, Istituto Italiano di Tecnologia, Viale Regina Elena 291, 00161, Rome, Italy

ARTICLE INFO

Handling Editor: Brian S Cummings

Keywords:
SARS-CoV-2
Protein-protein interactions
DNA aptamers
Inhibitors

ABSTRACT

The SARS-CoV-2 pandemic still poses a threat to the global health as the virus continues spreading in most countries. Therefore, the identification of molecules capable of inhibiting the binding between the ACE2 receptor and the SARS-CoV-2 spike protein is of paramount importance. Recently, two DNA aptamers were designed with the aim to inhibit the interaction between the ACE2 receptor and the spike protein of SARS-CoV-2. Indeed, the two molecules interact with the ACE2 receptor in the region around the K353 residue, preventing its binding of the spike protein. If on the one hand this inhibition process hinders the entry of the virus into the host cell, it could lead to a series of side effects, both in physiological and pathological conditions, preventing the correct functioning of the ACE2 receptor. Here, we discuss through a computational study the possible effect of these two very promising DNA aptamers, investigating all possible interactions between ACE2 and its experimentally known molecular partners. Our in silico predictions show that some of the 10 known molecular partners of ACE2 could interact, physiologically or pathologically, in a region adjacent to the K353 residue. Thus, the curative action of the proposed DNA aptamers could recruit ACE2 from its biological functions.

1. Introduction

Severe acute respiratory syndrome coronavirus 2 (SARS-CoV-2) is the causative agent of Coronavirus Disease 2019 (COVID-19) and it is responsible for the current pandemic, unfortunately still in progress [1,2]. Although the development of vaccines has led to excellent preventive effects of the disease [3], the development of new therapeutic molecules is still crucial to tackling the epidemic. Indeed, albeit the health emergency is now more tempered, COVID-19 infection is still largely present in the whole world, with nearly 600 million cases and 770.000 deaths.

To date, thanks to the knowledge of the molecular mechanisms the virus adopts for host cell entry, many approaches have been proposed to hinder the spread of the virus. Among the various possible therapeutic strategies against covid-19 disease, two are mostly proposed: (i) the vaccines, eliciting immune responses able to potently neutralize SARS-CoV-2 [4], and (ii) the identification of both small molecule and/or peptide inhibitors, acting to prevent the binding between the receptor-binding domain (RBD) of the SARS-CoV-2 glycosylated Spike protein and the cell surface receptors (ACE2) [5,6]. Intuitively, blocking RBD-ACE2 interaction can affect infection efficiency, the goal of most vaccines and neutralizing antibodies (nAbs) [7].

Despite the widely known role of small molecules to prevent the formation of protein-protein interactions (PPIs), traditionally they were not considered because the presence of a well-defined binding pocket on the protein surface is not always guaranteed [8]. However, small molecules could yield antiviral therapies more broadly active and less immunogenic. Moreover, small-molecule-based therapies are more controllable (better bio-distribution) than antibodies [9]. Indeed, specifically for COVID-19, an additional benefit of small molecules is the possibility of direct delivery into the respiratory system via inhaled or intranasal administration [8].

Of course, such kinds of therapies are not the only alternative. The design of short aptamers, typically defined as short single-chained oligonucleotides or peptides [10], to block the interaction between SARS-CoV-2 spike protein and ACE2 human receptor is another promising strategy [11]. Indeed, aptamers exhibit significant advantages with respect to protein therapeutics in terms of size, synthetic accessibility, and modification by medicinal chemistry [12].

* Corresponding author. Department of Physics, Sapienza University, Piazzale Aldo Moro 5, 00185, Rome, Italy.
E-mail address: edoardo.milanetti@uniroma1.it (E. Milanetti).

https://doi.org/10.1016/j.cbi.2023.110380
Received 20 August 2022; Received in revised form 22 January 2023; Accepted 1 February 2023
Available online 21 February 2023

Being the ACE2-RBD complex experimentally solved, the starting point of the development procedure is the ACE2 consecutive segment (peptide) that directly interacts with the corresponding molecular partner [13,14]. In particular, in most cases the inhibitory peptides are designed against Spike RBD [15–17], exploiting the knowledge of the ACE2 region that interacts with the spike protein (more specifically involving the residues at positions 21–40 and 76 [18]).

Symmetrically, it is possible to define an ACE2-binding peptide by considering the interacting region of Spike RBD consecutive in sequence. Such a strategy would have the benefit of being less influenced by the high mutational rate of the virus. Indeed, while the spike protein is subject to a high selective pressure [19], ACE2 is much more stable. In this scenario, in a recent work, Villa and coworkers have proposed two single-strand DNA molecules as possible aptamers for the inhibition of spike-ACE2 complex [20], where both aptamers interact with the region surrounding the K353 residue of the human receptor. Indeed, K353 is considered a key residue for the spike-ACE2 complex formation, since it directly interacts with the N501 residue of the spike RBD [21]. The interaction between the aptamer and this specific region of ACE2 has an inhibitory effect on the formation of the ACE2-RBD complex. Therefore, this work aims to investigate the possible undesired effect of two DNA aptamers proposed in Villa et al. [20].

The work of Villa et al. [20] is based on a mix of experimental, like SELEX, and computational, like molecular docking, approaches, where the resulting molecules represent powerful candidate drugs against SARS-CoV-2. Given the importance of these results, it could be fundamental to investigate the possible effect, in physiological and pathological conditions, of the binding between ACE2 and the candidate aptamers. Indeed, the aptamer binding on the K353 region could in principle interfere with the interactions between ACE2 and all its molecular partners. However, in such cases, the identified aptamers could also block the formation of functional protein-protein complexes involving ACE2 in physiological conditions. Hence, this work aims to investigate the possible undesired effect of two DNA aptamers proposed in Ref. [20]. Indeed, the interaction of the previously described molecules does not involve the spike protein of the virus but rather involves the ACE2 receptor. Therefore we believe that a discussion on the possible impairment of ACE2 functions following the interaction with the two candidate aptmas is necessary. To do so, we first selected the set of proteins that we know from experimental evidence interact with ACE2, calling them Molecular Partners (MP). We thus investigate if such interactions involve the regions interested in aptamers binding. As widely known, the prediction of the binding sites between two interacting proteins as well as the estimation of the three-dimensional conformation of the complex are still open problems of computational biology [22,23]. The idea of this work is to use a mix of computational approaches to discuss the possible interaction between the ACE2 receptor and its molecular partners in the interaction region between ACE2 and the aptamers developed for therapeutic purposes. To this end, more specifically, we adopted a molecular docking approach for estimating any ACE2-MP complexes. We moreover filtered the suggested poses using a shape complementarity evaluation of the putative interacting regions. To do it, we adopted a method we recently developed based on the formalism of 2D Zernike polynomials [24], which can provide the Binding Propensity (BP) for each residue of the two interacting proteins.

The advantage of combining the molecular docking approach with the analysis based on Zernike polynomials to evaluate the shape complementarity between interacting regions, allows to perform a screening of the poses proposed by the docking algorithm based on the van der Waals contribution which is known to play a crucial role in protein binding [25], as well as allows exploiting the speed of execution of the Zernike method which can thus be applied to many possible conformations [24]. The best ACE2-MP complexes obtained from the molecular docking procedure and characterized by high shape complementarity were selected and analyzed through short molecular dynamics simulations, to perform statistical analysis on inter-molecular contacts and refine the docking model. This computational study helps to clarify the possible effect of ACE2-spike interaction inhibitory molecules, analyzing how the binding between ACE2 and DNA aptamers could influence the interaction between ACE2 and other molecular partners. The paper is organized as follows. In the Results and Discussion section we describe each step of the analysis reported in this work. First of all, we describe the procedure for selecting the ACE2 molecular partners. Then we describe the molecular docking procedure and the method based on the Zernike formalism, in order to evaluate the shape complementarity between the molecular surfaces of the interacting proteins. Finally, we describe the procedure of molecular dynamics simulations and the corresponding obtained results. In Materials and Methods section we provide details on (i) the simulations performed, (ii) the molecular docking, (iii) the evaluation of the molecular surface complementarity through descriptors based on Zernike formalism, and (iv) the procedure for the hydrophaty profile calculation.

2. Results and discussion

2.1. Selection of the molecular partners of ACE2

Firstly, we need to identify all the protein-protein interactions where ACE2 is involved. Indeed, using Uniprot database [26] (as well as confirming the information on other DBs available in the literature, such as [27]) we have determined the proteins with experimental evidence of direct interaction with the human ACE2 receptor (UniProt code: Q9BYF1).

The list of 10 molecular partners of ACE2 we identified is reported in the following list. Indeed, according to our analysis human ACE2 can interact with:

- Angiotensinogen (UniProt code: P01019, gene: AGT), a glycoprotein produced mainly in the liver, that is the sole precursor of all angiotensin peptides, playing, therefore, a key role in the renin-angiotensin system [28].
- Excitatory amino acid transporter 5 (UniProt code: O00341, gene: SLC1A7), a protein, expressed mainly in the retina, that recognizes with high-affinity L-glutamate (excitatory amino acid), allowing the conduction of chloride ions [29].
- Transmembrane protease serine 2 (UniProt code: O15393, gene: TMPRSS2), a membrane-anchored serine protease involved in the physiologic function of the prostate [30]. It has been shown that this protein can promote SARS-CoV-2 infection. This protease can perform the proteolytic cleavage of ACE2, necessary for the viral uptake, and the cleavage of spike protein [31,32].
- Kininogen-1 (UniProt code: P01042, gene: VKNH1), a precursor protein that can generate High molecular weight kininogen (HMWK), is essential for blood coagulation, and low molecular weight kininogen. In addition, HMWK release a peptide, bradykinin, with numerous physiological effects [33]. Interestingly, when SARS-CoV-2 infection reduces the levels of ACE2, it increases the concentration of a bioactive metabolite of bradykinin, associated with lung injury and inflammation [34].
- Vitronectin (UniProt code: P04004, gene: VNT), a glycoprotein that can be found in blood, extracellular matrix, and bone. It is recognized by some integrins working as a cell-to-substrate adhesion molecule. In addition, it inhibits the membrane-damaging effect of the terminal cytolytic complement pathway [35,36].
- Integrin beta-1 (UniProt code: P05556, gene: ITB1), is a cell surface receptor. It can form complexes with an integrin alpha protein to form integrin complexes, to work as receptors of several compounds, such as collagen [37].
- Neurotensin/neuromedin N (uniprot code: P30990, gene: NEUT). Neurotensin is a 13 amino acid neuropeptide, synthesized as part of a larger precursor that also contains neuromedin N, a six amino acid

peptide. Neurotensin is important in the regulation of fat metabolism [38].

- Defensin-5 (UniProt code: Q01523, gene: DEFA5), is the main member of a family of microbicidal proteins that control the microbiota composition [39].
- Sodium-dependent neutral amino acid transporter B(0)AT1 (UniProt code: Q695T7, gene: SLC6A19), is a transporter that is necessary for the reabsorption of neutral amino acids in renal and intestinal cells. In intestine, it requires ACE2 for expression and transporter activity [40,41].
- C-type lectin domain family 4 member M (UniProt code: Q9H2X3, gene: CLEC4M), a receptor involved in pathogen recognition in liver [42]. Interestingly, it has been proposed as an attachment receptor for SARS-CoV [43].

An ACE2-interacting drug can in principle interfere with all these suggested protein-protein interactions. Here we focused on the two aptamers proposed by Villa et al. [20], whose ACE2 binding region is centered around residue K353. In Fig. 1 we show two examples of molecular docking between ACE2 and its MPs. In the next sections, we investigated the ACE2 region most probable involved in the complex with each of these possible interactors, explaining the rationale for the selection of MP prone to interact in the K353 region.

2.2. Selection of protein complexes involving ACE2: molecular docking and Zernike-based binding propensity

In the previous section, we reported experimental information generating the list of proteins that interact with the ACE2 receptor. However, to the best of our knowledge, no experimental information is available regarding the region of ACE2 where the molecular interaction takes place.

Hence, we designed a fully computational procedure intending to propose: (i) the ACE2 protein interactors that bind ACE2 in the region of K353 residue, (ii) the corresponding poses provided by molecular docking, and (iii) an evaluation of the binding properties through short molecular dynamics simulations. In particular, a combination of several computational techniques was used to address the first of these three steps. As said, if a molecular interactor binds in the neighborhood of K353, such interaction could be hampered by the two aptamers designed in Villa et al. [20]. Therefore, we split the computational procedure into several phases and we reported our results in Fig. 2.

First of all, we modeled the structure of each MP (not known experimentally) using AlphaFold-2 [44], currently the best available method for protein structure prediction [45]. Analyzing the protein structures of the two interacting proteins (ACE2 and its molecular partners), we evaluated the shape complementarity between protein regions applying our recently developed method, based on the mathematical formalism of Zernike polynomials [24]. Thus, we were able to identify regions of the ACE2 molecular surface with high shape complementarity with any other region of each of the 10 MP. In this way we can identify, for each ACE2-MP pair, the regions of ACE2 that are more prone to bind, since the higher the shape complementarity, the greater the probability to have a binding mediated by van der Waals forces [25]. Using the Zernike-based description, we defined the *binding propensity*, a residue-level descriptor indicating the tendency of each residue to interact with a specific protein. In particular, we compare each patch of the ACE2 receptor with each other patch of the corresponding MP and assign to each patch the value of minimum distance obtained by comparing all patches. Since each patch is centered on each surface point, multiple patches are attributed to each residue of each protein. At the end of this procedure, the minimum distance values between all the surface points belonging to each residue are averaged for the definition of the Binding Propensity (see Ref. [24] for more details). In the top panels of Fig. 2a–d, we reported the binding propensity for four of the possible ACE2 MPs. In addition, we perform a docking simulation for each ACE2-MP pair using the ZDOCK method [46]. We selected in each case the ten best docking poses, according to the ZDOCK score.

For each docking pose, we select the ACE2 residues interacting with the molecular partner (i.e. the residues of the ACE2 binding site), in accordance with a threshold value on the distance between the C_α atoms (see Methods). Indeed, in the central plot of Fig. 2a–d we show the minimum distance between ACE2 C_α and the closest MP C_α. These plots regard some docking poses of 3 ACE2-MP pairs.

Finally, we also check the reliability of the structural prediction

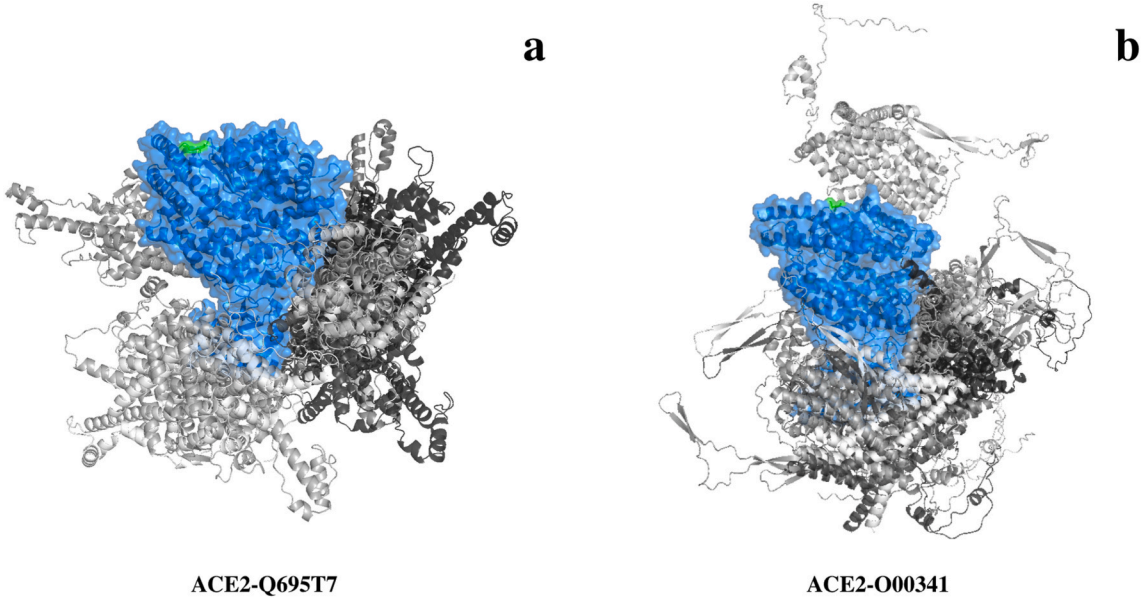

Fig. 1. Molecular docking results. a) Molecular representation of the different poses obtained for the human ACE2-Q695T7 complex. ACE2 molecular surface is colored in blue and the K353 residue of ACE2 is highlighted in green. Cartoon representations of Q695T7 protein with different shades of gray show the different poses provided by the docking algorithm. In all poses, the green region is not directly involved in the binding. **b)** Same as in a), but for human ACE2-O00341 complex. In this case, one pose involves the marked region.

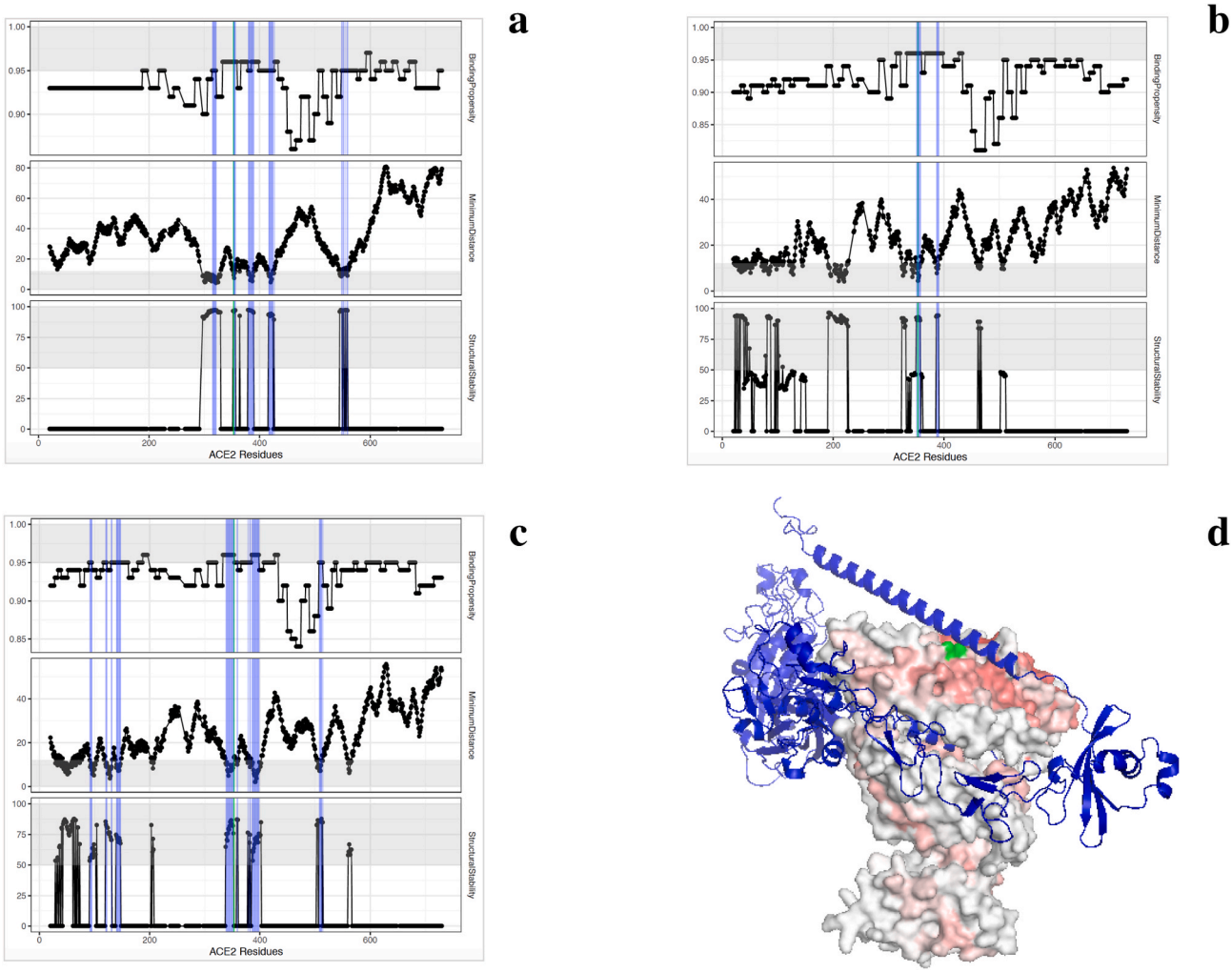

Fig. 2. Selection of the best docking poses. a) From top to bottom, binding propensity scores for each residue of the ACE2 protein to binding its corresponding molecular partner (UniProt code: O00341); minimum distance between each residue of the ACE2 protein and any of the residue of its MP; and the AlphaFold reliability score for the residues found in contact. Blue shaded regions mark the residues found in contact in the selected docking pose, while the green shaded region highlights the target region of [20]. **b)** Same as in panel a) but for ACE2 protein vs MP, uniprot code: P05556. **c)** Same as in panel a) but for ACE2 protein vs MP, uniprot code: P30990. **d)** Molecular surface representation of human ACE2 and cartoon representation of P05556 (blue). The surface is colored according to the binding propensity score.

provided by the AlphaFold-2 algorithm. Indeed, AlphaFold-2 provides a reliability score of its prediction for each residue. We report in the bottom panels of Fig. 2a–d the reliability score of AlphaFold-2 for the MP residues found in contact with ACE2. The higher the score, the more the binding region is well structured. Regions predicted as highly unstructured by the algorithm have to be discarded, since our approach based on Zernike polynomials evaluates the shape complementarity between two regions with a well-defined structure. More specifically, for each residue of ACE2, we calculate the average of the AlphaFold-2 descriptor over all interacting residues of the MP, to know if each residue of the binding site of ACE2 is interacting with a well-structured region (structural stability descriptor > 50) of the partner.

We thus combined all these analyses to identify the MP that most probably interacts in the K353 region. Indeed, first of all, we select the MP characterized by a high binding propensity with ACE2 in the K353 region. Moreover, these MPs must have almost one of the docking pose where the ACE2 binding region is close to K353. Finally, the interacting region has to be properly folded, according to the AlphaFold-2 reliability score.

Considering these constraints, we selected 3 MP as potential interactors in the region of K353 and we reported them in Fig. 2 (analyzes of all other systems that were not selected in this work are reported in the Supplementary Information, SI). To better understand the output of this procedure, in Fig. 2-d we report the molecular surface of the ACE2 receptor in complex (predicted by molecular docking) with one of its partners. The molecular surface of ACE2 is colored in accordance with the binding propensity of each portion of the molecular surface: the higher the binding propensity, the greater the intensity of the red color.

The 3 MP selected are Excitatory amino acid transporter 5 (UniProt code: O00341), Integrin beta-1 (P05556), and Neurotensin/neuromedin N (P30990). In this study, we add a further system (UniProt code: P01019) whose binding between ACE2 and the MP occurs in a region that does not involve the K353 residue of ACE2. The purpose of this additional system is to compare the properties of molecular systems whose interactions involve the K353 residue from a case that does not have this characteristic. In the following sections, we analyze the results of the molecular dynamics simulation performed for such complexes.

2.3. *Molecular dynamics simulation for each selected complex*

For each of the four selected ACE2-interactor complexes, we performed a 100 ns long molecular dynamics simulation. The aim of this procedure is both to refine the predicted docking model [47,48] and to statistically study the structural stability of the estimated complex by

analyzing the inter-molecular interactions during the simulation. Indeed, the greater the stability of the interaction between the ACE2 receptor and the corresponding molecular partner (each of the 4 selected), the greater the probability that the two macromolecules interact with high-affinity [16,25]. For this purpose, we first calculate two descriptors that provide information on the mobility of each system: the Root Mean Square Deviation (RMSD) and Root Mean Square Fluctuation (RMSF). The first descriptor reports the deviation of the atomic positions between each structure related to each frame of the trajectory and a reference structure (usually, as also, in this case, the starting structure is considered). On the other hand, the second descriptor evaluates the average fluctuation of each residue, allowing us to distinguish the more mobile regions from the more stable ones of the analyzed complex. The analysis of the RMSD, shown in Fig. 3a, was carried out by fitting the structures of the entire complex onto the ACE2 receptor since it is the molecule in common to all the molecular systems analyzed. To evaluate the binding effect with each molecular partner, four RMSD curves were calculated: (i) the RMSD of the entire ACE2

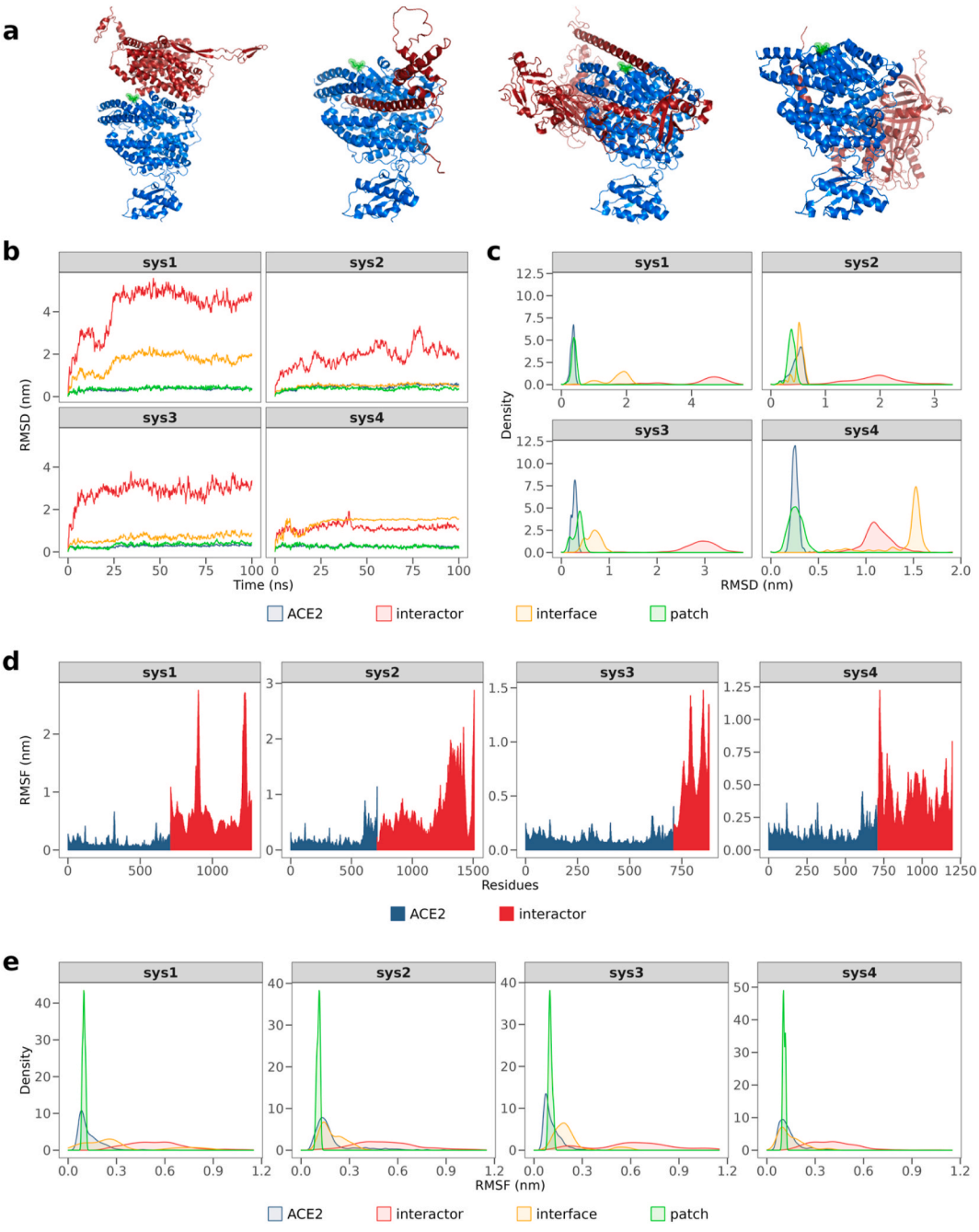

Fig. 3. RMSD and RMSF analysis by fitting the system on the ACE2 receptor. a) Cartoon representation of the 4 selected systems. The ACE2 receptor is shown in blue, its molecular partner in red and the ACE2 residue 353 in green. **b)** RMSD values as a function of time. In blue is the RMSD of ACE2, in red is the RMSD of the molecular partner, in yellow is the RMSD of the interface, and in green the RMSD of the patch centered in the K353 residue of the ACE2 receptor. **c)** RMSD distributions of each system. In blue is the RMSD distribution of ACE2, in red the RMSD distribution of the molecular partner, in yellow is the RMSD distribution of the interface, and in green is the RMSD distribution of the patch centered in the K353 residue of the ACE2 receptor. **d)** RMSF for any residue of each molecular system. In blue and in red the RMSF of the residues belonging to ACE2 and molecular partner, respectively. **e)** RMSF distributions of each system. In blue is the RMSF distribution of ACE2, in red the RMSF distribution of the molecular partner, in yellow is the RMSF distribution of the interface, and in green is the RMSF distribution of the patch centered in the K353 residue of the ACE2 receptor.

structure, (ii) the RMSD of the entire molecular partner structure (MP), (iii) the RMSD of the two interfaces of the complex and (iv) the RMSD of the region around the K353 residue of ACE2 receptor. After an initial transient phase, we note that after about 30 ns all simulated systems reach equilibrium, allowing us to study the distributions of RMSD for the phase in which the system is at equilibrium (lower part of Fig. 3a). Not surprisingly, the RMSDs of all ACE2-interacting proteins is greater than the RMSDs of ACE2 itself. Indeed, this is certainly since the whole system is fitted only on ACE2. Furthermore, the ACE2 receptor structure is experimentally resolved, while the structures considered for the 4 MPs are predicted with the AlphaFold-2 algorithm, which may need further refinement through molecular dynamics simulations. A more surprising result, on the other hand, is shown when we consider the distributions of the RMSD values in the structural equilibrium phase of each trajectory. In all systems, the standard deviation of the RMSD values of the entire structure interacting with ACE2 is greater than the standard deviation of ACE2 (see Table 1).

To better investigate the binding between the macromolecule pairs, we also consider both the binding interface (defined by the two binding sites of the two interacting proteins) and the region around the K353 residue of the ACE2 receptor (which is defined by the residues whose alpha carbons have a distance less than 8Å from with the alpha carbon of residue 353). For system 4 (UniProt code: P01019) the RMSD of the interface is on average higher than the RMSD of the whole interacting protein. Conversely, the patch centered in ACE2 residue K353 is particularly stable. Since the MP of system 4 does not interact with the K353 residue of the ACE2 receptor, this result would suggest the stability of the region centered in the K353 residue regardless of the binding with the molecular partner. Therefore, the region centered in the K353 residue is less fluctuating than the other binding and non-binding residues.

The most interesting case concerns system 2 (UniProt code: P05556) as the RMSD of the patch centered in 353 is more stable than both the interface and the whole structure of ACE2 (see Table 1). The analysis of the RMSF (Fig. 3b) is instead specific residue, allowing us to consider

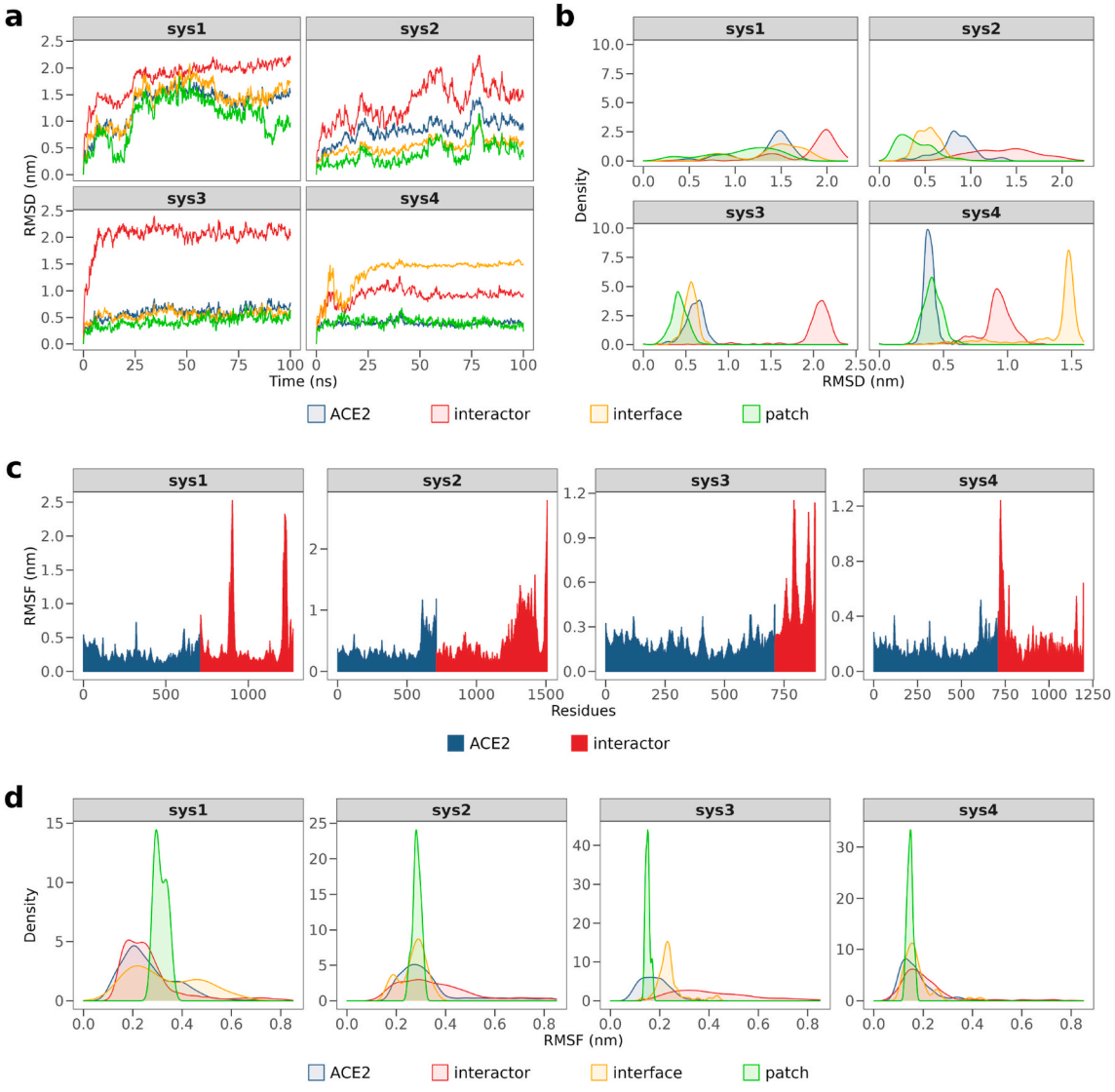

Fig. 4. RMSD and RMSF analysis by fitting the system on the whole molecular system. a) RMSD values as a function of time. In blue is the RMSD of ACE2, in red is the RMSD of the molecular partner, in yellow is the RMSD of the interface, and in green the RMSD of the patch centered in the K353 residue of the ACE2 receptor. **b)** RMSD distributions of each system. In blue is the RMSD distribution of ACE2, in red the RMSD distribution of the molecular partner, in yellow is the RMSD distribution of the interface, and in green is the RMSD distribution of the patch centered in the K353 residue of the ACE2 receptor. **c)** RMSF for any residue of each molecular system. In blue and in red the RMSF of the residues belonging to ACE2 and molecular partner, respectively. **c)** RMSF distributions of each system. In blue is the RMSF distribution of ACE2, in red the RMSF distribution of the molecular partner, in yellow is the RMSF distribution of the interface, and in green the RMSF distribution of the patch centered in the K353 residue of the ACE2 receptor.

how much each residue fluctuates during the simulation of MD. The analysis confirms that residues belonging to ACE2 partners are generally more fluctuating than residues belonging to the ACE2 receptor. However, especially for systems 1 and 2, the patch centered in K353 is particularly stable (more stable than the interface and more stable than the ACE2 receptor) as shown in Table 1. ACE2 is the molecule in common to all systems analyzed in this work, therefore in Fig. 3, we have shown the results related to the fit of the entire molecular system on the ACE2 receptor, thus allowing us to quantify how much each MP fluctuates with respect to ACE2. Obviously, by construction, in this first analysis ACE2 receptor will be more rigid than the corresponding molecular partner but, on the other hand, this procedure allows us to compare the atomic mobility of the 4 molecular partners with each other.

Despite the importance of this first analysis, we show in Fig. 4 the same analyzes but considering the fit on the whole system (ACE2-partner complex), so that we can better quantify (and compare) the motion of every single part of the system: (i) the ACE2, (ii) the MP, (iii) the interface between the two proteins and (iv) the patch centered around the K353 residue of the ACE2 receptor. Typically, also, in this case, the ACE2 receptor is more stable, showing greater rigidity than any corresponding molecular partner (see Table 2). In particular, the proteins interacting with ACE2 have some more fluctuating residues (which are characterized by a high RMSF value, as shown in Fig. 4-b), having values in a range from 5 to 25 Å.

Interestingly, we note that for the first three systems analyzed (UniProt code: O00341, P05556, and P030990) the binding interface is typically more stable, in terms of RMSD, than the two single proteins (ACE2 and the molecular partner). In contrast, system 4 (UniProt code: P01019), which is defined as a control because the partner does not interact with the K353 residue of the ACE2 receptor (according to our computational predictions), is characterized by a very mobile binding interface (13.50 ± 2.70 Å) and the RMSD of the entire ACE2 system (3.91 ± 0.47 Å) is comparable with the RMSD of the patch centered around the K353 residue (4.14 ± 0.75 Å). However, we note that this system is characterized by a very compact binding interface, as shown by the gyration radius analysis in Fig. S2, which is calculated considering all residues belonging to the two interacting regions. On the contrary, the systems 1 and 2 are characterized by gyration radius value higher than the other two systems. In order to verify the reliability of the results, we performed a molecular dynamics replica for each analyzed system. In particular, for each of the 4 systems we perform a new 100 ns long molecular dynamics simulation. Both RMSD and RMSF values are compatible between the two sets of simulations. The values of both the RMSD comparisons (see Table 1 of SI) and the RMSF correlations (0.77, 0.72, 0.89 and 0.61 for the system 1, system 2, system 3 and system 4, respectively) are shown in the Supplementary Information (see Fig. S3).

Table 1
Mean values with the corresponding standard deviations of RMSD and RMSF for each system, obtained by fitting the entire molecular system onto ACE2 receptor.

system	UniProt code	part	mean RMSD (Å)	sd RMSD (Å)	mean RSMF (Å)	sd RSMF (Å)
1	O00341	ACE2	3.39	0.63	1.32	0.78
1	O00341	interactor	41.88	10.28	6.98	5.02
1	O00341	interface	16.64	4.28	3.17	2.44
1	O00341	patch	3.83	0.81	0.98	0.08
2	P05556	ACE2	4.72	1.12	1.93	1.40
2	P05556	interactor	18.99	4.89	7.48	4.91
2	P05556	interface	5.19	0.88	1.94	0.72
2	P05556	patch	3.71	0.70	1.08	0.09
3	P30990	ACE2	2.70	0.50	1.09	0.49
3	P30990	interactor	28.69	4.52	6.98	3.30
3	P30990	interface	6.63	1.55	2.17	1.19
3	P30990	patch	3.36	1.05	1.03	0.11
4	P01019	ACE2	2.53	0.36	1.30	0.63
4	P01019	interactor	11.28	1.67	4.14	1.65
4	P01019	interface	13.98	2.71	1.47	0.76
4	P01019	patch	2.62	0.72	1.07	0.07

Table 2
Mean values with the corresponding standard deviations of RMSD and RMSF for each system, obtained by fitting the entire molecular system onto the entire system (which is composed of ACE2 and its molecular partner).

system	uniprot code	part	mean RMSD (Å)	sd RMSD (Å)	mean RMSF (Å)	sd RMSF (Å)
1	O00341	ACE2	13.17	3.35	2.63	1.10
1	O00341	interactor	18.19	3.30	4.16	4.73
1	O00341	interface	13.85	3.76	3.28	1.39
1	O00341	patch	10.68	3.86	3.13	0.25
2	P05556	ACE2	8.40	2.14	3.51	1.80
2	P05556	interactor	13.52	3.65	5.08	3.74
2	P05556	interface	5.39	1.35	2.68	0.53
2	P05556	patch	3.92	1.95	2.84	0.16
3	P30990	ACE2	5.98	1.14	1.79	0.60
3	P30990	interactor	20.35	2.46	4.86	2.43
3	P30990	interface	5.51	0.83	2.40	0.57
3	P30990	patch	4.23	0.98	1.51	0.09
4	P01019	ACE2	3.91	0.47	1.70	0.70
4	P01019	interactor	9.11	1.39	2.30	1.76
4	P01019	interface	13.50	2.70	1.76	0.64
4	P01019	patch	4.14	0.75	1.47	0.11

Additional analysis for evaluating the role of hydrogen bonds at the interface was also conducted for all 4 simulated systems. In particular, we defined for each system the distribution of the number of hydrogen bonds between the interacting residues of the two proteins. Analyzing the entire trajectory of each system, we obtain a single distribution for each ACE2-MP system. We note that system 2 and system 4 are characterized by a higher number of H-bonds than the other two systems (Fig. 5-a). The average number of hydrogen bonds is 9.00 ± 2.47 and 8.98 ± 3.29 for systems 2 and 4 respectively. The variance of the system 4 distribution is higher than the variance of system 2, suggesting that system 4 can adopt different types of poses during the simulation (since from 5 to 12 hydrogen bonds there is approximately the same probability). Furthermore, we note that in system 1 the number of hydrogen bonds does not play a predominant role, because the mean value of the number of hydrogen bonds is 0.25. To better investigate the role of the ACE2 receptor in the possible binding with its corresponding molecular partners, we analyze how many contacts each residue of ACE2 establishes with the residues of the partner Fig. 5-b. In particular, to consider side chain packaging, for this analysis, we define contact between two residues if the distance between the centroids of their side chains is less than 15Å. Also in this case the simulated system 2 is remarkably interesting. In fact, as shown in Fig. 5-b, system 2 has many residues with a high number of contacts, and the K353 residue is widely involved in binding with the molecular partner. More specifically, the ACE2 residues in system 2 have on average 6.13 interacting residues belonging to the corresponding MP. On the other hand, the other three systems have a very similar average number of contacts for each residue: 4.50, 4.40, and 4.64 for systems 1, 3, and 4 respectively.

2.4. Hydropathy compatibility between the two binding sites of each ACE2-MP system

It is known that the balance between hydrophilicity and hydrophobicity in the binding regions plays a primary role in the recognition and interaction between two proteins [25,49]. Therefore, a quantification of both the hydrophilic and hydrophobic contribution, and therefore of the entire hydropathy profile, is useful to better characterize the interaction between two proteins. However, when we consider the molecular complex (in this case the interaction between ACE2 and each of its molecular partners) the two binding sites have no direct interaction with water molecules, as hydration water is excluded to favor the interaction

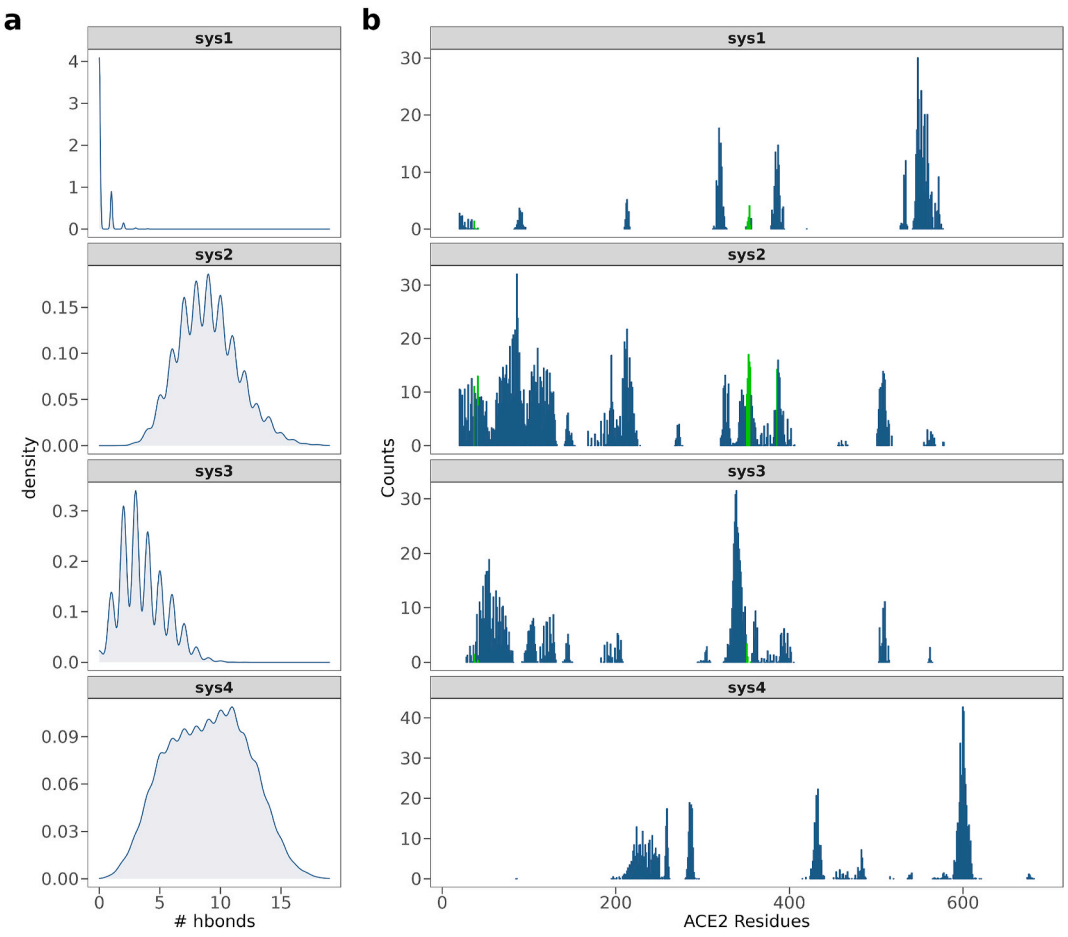

Fig. 5. Contact analysis at the binding interface. a) Distributions of the number of H-bonds at the binding interface for each of the 4 molecular systems composed of the ACE2 receptor and the corresponding molecular partner. **b)** For each residue of the ACE2 receptor the mean value of the number of its interacting residues belonging to the corresponding molecular partner is reported. The residues belonging to the patch centered on the K353 residue of the ACE2 receptor are highlighted in green.

between the two proteins. In order to evaluate the hydropathy properties of the two binding sites, it is therefore necessary to split the two proteins and analyze the two structures separately, alone in solution, focusing the analysis on the water molecule disposition around the two binding sites. Here, we select the most representative structures of each ACE2-MP system, extracting from the molecular dynamics simulation of each system the conformation of the ACE2-MP complex with the RMSD vale closest to the mean RMSD value in the equilibrium phase of the simulation. For each selected structure, both of ACE2 and of MP, we perform a 10 ns long molecular dynamics simulation in order to analyze the arrangement of water molecules around each binding region. The idea is to define the hydrophilic and hydrophobic properties of the interfaces in their bound conformation, since 10 ns is too short to expect large conformational changes but sufficient to perform statistical analysis on the motion of hydration water molecules. More specifically, we describe the hydrophilicity and hydrophobicity properties by measuring the orientation of water molecules (analysing the orientation of the hydrogen bonds among water molecules) in first and second hydration shells respectively, as shown in Refs. [50,51]. The analysis shows a high correlation between the histograms obtained from the interacting regions (see Fig. S4 of SI) belonging to ACE2 and the corresponding MP respectively. In particular, in agreement with the results obtained in the analysis of the number of H-bonds, system 2 has a higher correlation value (the Pearson coefficient is 0.93) between the two histograms describing the hydropathy profile of the two interfaces, highlighting a high level of compatibility both hydrophilic and hydrophobic.

3. Conclusions

In this pandemic scenario, a great effort is being spent to identify possible drugs that could prevent SARS-CoV-2 infection [52]. Therefore, it is worth noting that such a study can be generalized to any type of proposed ACE2-interacting molecule. In general terms, just as it is of fundamental importance to have possible drug candidates capable of inhibiting the interaction between ACE2 and the spike protein of SARS-CoV-2, it is equally essential to consider the possible side effects if the candidate drug interacts directly with the ACE2 receptor. Specifically, here we discussed the possible effect of two DNA aptamers recently proposed by Villa et al. [20] which interact with the ACE2 receptor through the region around the K353 residue. We, through a mix of computational approaches, have analyzed the possible molecular complexes composed of ACE2 and its molecular partners which, according to computational calculations, would involve the K353 residue. Among the ten proteins for which it is known from experimental evidence to interact with the ACE2 receptor both in physiological and pathological conditions, we have selected 3 proteins that could interact with ACE2 involving the region centered around the K353 residue. In this work, we report the details of the analyzes obtained from short molecular dynamics simulations of the models predicted by molecular docking. The three selected systems have a stable binding interface with respect to the rest of the molecular system. In particular, the patch centered on residue 353 appears to have low atomic mobility, regardless of the interaction with the molecular partner. Interestingly, system 2 analyzed in this work (UniProt code of the MP: P05556) is not only

characterized by high interface stability but also has a high number of hydrogen bonds between the two interacting proteins, as well as the highest number of residues interacting with the partner adjacent to residue K353. Our analysis suggests the importance of further investigating the interactions between ACE2 and its molecular partners, as such structures are not yet known experimentally. This information can help us to clarify the possible adverse effects due to the interaction between ACE2 and molecule able to inhibit its binding with the SARS-CoV-2 spike protein. Indeed, these findings may have both implications of a more theoretical nature and of a more practical one. On the one hand, if confirmed also by experimental tests, this approach could become a well-defined computational procedure useful for the determination of the binding regions between two interacting proteins, combining molecular docking methods with the algorithm based on Zernike polynomials that we have recently developed. On the other hand, more importantly, we could evaluate the effect that DNA aptamer candidates can have, both in physiological and pathological conditions, in the interaction with ACE2 receptor. This approach, which in principle can also be applied to other molecular systems, plays a primary role in the identification of the molecular mechanisms which would lead to possible side effects for candidate molecular inhibitors.

4. Materials and methods

4.1. Molecular dynamics simulations

All simulations were performed using Gromacs [53]. Topologies of the system were built using the CHARMM-36 force field [54]. The protein was placed in a dodecahedric simulative box, with periodic boundary conditions, filled with TIP3P water molecules [55]. For all simulated systems, we checked that each atom of the proteins was at least at a distance of 1.1 nm from the box borders. Each system was then minimized with the steepest descent algorithm. Next, a relaxation of water molecules and thermalization of the system was run in NVT and NPT environments each for 0.1 ns at 2 fs time-step. The temperature was kept constant at 300 K with v-rescale thermostat [56]; the final pressure was fixed at 1 bar with the Parrinello-Rahman barostat [57].

LINCS algorithm [58] was used to constraint bonds involving hydrogen atoms. A cut-off of 12 Å was imposed for the evaluation of short-range non-bonded interactions and the Particle Mesh Ewald method [59] for the long-range electrostatic interactions. The described procedure was used for all the performed simulations.

4.2. Molecular docking protocol and interface definition

Molecular docking between ACE2 receptor and any of its molecular partners has been performed using ZDOCK software [46]. Starting from the docking resulting structures, we performed 100 ns of MD simulation both to refine the docking poses and to perform statistical analysis on inter-molecular contacts. For each analyzed complex, the interface was defined by taking ACE2 and MP residues whose α-carbons have a distance lower than 12 Å. Furthermore, when we want to analyze side chain orientation, we set the threshold value of the distance between the two side chain centroids to 8.5 Å [19].

4.3. Molecular surface complementarity via Zernike descriptors

For each protein, we calculate its molecular surface using DMS software [60]. Then, we extracted any portion of the protein surface (so defining the patches of the surface) and, with a voxelization procedure, we represent the protein patch as a 3D function. Starting from this function, we pass from a 3D representation to a 2D representation with a recently developed protocol [24]. This final 2D function can be described as a series expansion on the basis of the 2D Zernike Polynomials [24,61].

More specifically, given a function $f(r, \varphi)$ (polar coordinates) defined inside the region $r < 1$ (unitary circle), it is possible to represent the function in the Zernike basis as

$$f(r,\varphi) = \sum_{n=0}^{\infty} \sum_{m=0}^{m=n} c_{nm} Z_{nm} \tag{1}$$

with

$$c_{nm} = \frac{(n+1)}{\pi} \langle Z_{nm} | f \rangle = \frac{(n+1)}{\pi} \int_0^1 dr r \int_0^{2\pi} d\varphi Z^*_{nm}(r,\varphi) f(r,\varphi). \tag{2}$$

being the expansion coefficients. The Zernike polynomials are complex functions, composed by a radial and an angular part,

$$Z_{nm} = R_{nm}(r) e^{im\varphi}. \tag{3}$$

where the radial part for a certain couple of indexes, n and m, is given by

$$R_{nm}(r) = \sum_{k=0}^{\frac{n-m}{2}} \frac{(-1)^k (n-k)!}{k! \left(\frac{n+m}{2}-k\right)! \left(\frac{n-m}{2}-k\right)!} r^{n-2k} \tag{4}$$

In general, for each couple of polynomials, one finds that

$$\langle Z_{nm} | Z_{n'm'} \rangle = \frac{\pi}{(n+1)} \delta_{nn'} \delta_{mm'} \tag{5}$$

which ensures that the polynomials can form a basis.

Taking the norm of the expansion coefficients we deal with an ordered set of numerical descriptors that compactly summarize the shape of the examined molecular surface. The precision of the description can be selected by modifying the order of the expansion N. In this work, we fix N = 20, corresponding to 121 numerical descriptors representing each function.

The shape complementarity between two surfaces can be easily evaluated by applying a metric between the two vectors of numbers describing them [24,62–64]. Indeed, we adopted the euclidean distance. When two surfaces have a low distance between them, they are characterized by a similar shape and therefore they are suitable for binding. Using this approach we are able to identify with a promising performance the papable binding regions between two interacting proteins.

4.4. Hydropathy compatibility characterization

We have adopted the method described in Ref. [51]. The procedure is based on the calculation of the conditional probability density of finding a water molecule with a specific orientation, given its distance from the nearest atom of the solute [50,65]. To this end we have selected the mean structures of each ACE2-MP simulation, where for each system the mean structure is defined as the frame with RMSD closest to the mean RMSD, which is calculated on the equilibrium phase of each simulation. Therefore, we identify 4 average structures, one for each ACE2-MP system. We split each identified complex in order to separate the ACE2 structure from the structure of the corresponding molecular partner. For both structures we perform a 10 ns long molecular dynamics simulation, in order to statistically investigate the rearrangement of water molecules around the two binding sites (which interact with water molecules when proteins are considered alone in solution). Through the procedure described in Ref. [51], we calculate the orientation of the hydrogen bonds of the water molecules in the first and second shell of hydration, thus defining the conditional probability density for each binding site. Therefore, we can easily compare each conditional probability density profile of the ACE2 binding site with the conditional probability density profile related to the binding site belonging to the corresponding molecular partner.

Author statement

G.R. and E.M. conceived the research. E.M,

M.M. and L.D.R. selected the molecular interactors and retrieved the structures.

E.M. and L.B. performed the molecular dynamics simulations and analyzed the data.

M.M. and L.D.R carried out additional statistical analyzes.

All authors wrote and revised the manuscript.

Code availability

All codes used to produce the findings of this study are available from the corresponding author upon request. The code for the Zernike algorithm is available at https://github.com/matmi8/Zernike2D.

Competing interests

The authors declare no conflict of interest.

Declaration of competing interest

The authors declare that they have no known competing financial interests or personal relationships that could have appeared to influence the work reported in this paper.

Data availability

Data will be made available on request.

Acknowledgements

The research leading to these results has been also supported by European Research Council Synergy grant ASTRA (n. 855923).

Appendix A. Supplementary data

Supplementary data to this article can be found online at https://doi.org/10.1016/j.cbi.2023.110380.

References

[1] Bhupender S. Chhikara, Brijesh Rathi, Jyoti Singh, F.N.U. Poonam, Corona virus sars-cov-2 disease covid-19: infection, prevention and clinical advances of the prospective chemical drug therapeutics, Chem. Biol. Lett. 7 (1) (2020) 63–72.

[2] Salim S Abdool Karim, Tulio de Oliveira, New sars-cov-2 variants—clinical, public health, and vaccine implications, N. Engl. J. Med. 384 (19) (2021) 1866–1868.

[3] Seyed M. Moghadas, Thomas N. Vilches, Kevin Zhang, Chad R. Wells, Affan Shoukat, Burton H. Singer, Lauren Ancel Meyers, Kathleen M. Neuzil, Joanne M. Langley, Meagan C. Fitzpatrick, et al., The impact of vaccination on coronavirus disease 2019 (covid-19) outbreaks in the United States, Clin. Infect. Dis. 73 (12) (2021) 2257–2264.

[4] Wilfredo F. Garcia-Beltran, Evan C. Lam, Kerri St Denis, Adam D. Nitido, Zeidy H. Garcia, Blake M. Hauser, Jared Feldman, Maia N. Pavlovic, David J. Gregory, Mark C. Poznansky, et al., Multiple sars-cov-2 variants escape neutralization by vaccine-induced humoral immunity, Cell 184 (9) (2021) 2372–2383.

[5] Nicholas J. Matheson, Paul J. Lehner, How does sars-cov-2 cause covid-19? Science 369 (6503) (2020) 510–511.

[6] Jian Shang, Yushun Wan, Chuming Luo, Gang Ye, Qibin Geng, Ashley Auerbach, Fang Li, Cell entry mechanisms of sars-cov-2, Proc. Natl. Acad. Sci. USA 117 (21) (2020) 11727–11734.

[7] Wanbo Tai, He Lei, Xiujuan Zhang, Jing Pu, Denis Voronin, Shibo Jiang, Yusen Zhou, Lanying Du, Characterization of the receptor-binding domain (rbd) of 2019 novel coronavirus: implication for development of rbd protein as a viral attachment inhibitor and vaccine, Cell. Mol. Immunol. 17 (6) (2020) 613–620.

[8] Damir Bojadzic, Oscar Alcazar, Jinshui Chen, Sung-Ting Chuang, Jose M Condor Capcha, Lina A. Shehadeh, Peter Buchwald, Small-molecule inhibitors of the coronavirus spike: ace2 protein–protein interaction as blockers of viral attachment and entry for sars-cov-2, ACS Infect. Dis. 7 (6) (2021) 1519–1534.

[9] Damir Bojadzic, Peter Buchwald, Toward small-molecule inhibition of protein–protein interactions: general aspects and recent progress in targeting costimulatory and coinhibitory (immune checkpoint) interactions, Curr. Top. Med. Chem. 18 (8) (2018) 674–699.

[10] Fatma Söylemez, Çağatay Han Türkseven, Aptamers and possible effects on neurodegeneration, in: Neuroprotection-New Approaches and Prospects, IntechOpen, 2019.

[11] Xiaoqiang Huang, Robin Pearce, Yang Zhang, De novo design of protein peptides to block association of the sars-cov-2 spike protein with human ace2, Aging (Albany NY) 12 (12) (2020), 11263.

[12] Anthony D. Keefe, Supriya Pai, Andrew Ellington, Aptamers as therapeutics, Nat. Rev. Drug Discov. 9 (7) (2010) 537–550.

[13] Yanxiao Han, Petr Král, Computational design of ace2-based peptide inhibitors of sars-cov-2, ACS Nano 14 (4) (2020) 5143–5147.

[14] Shravan B. Rathod, B Prajapati Pravin, Lata B. Punjabi, Kuntal N. Prajapati, Neha Chauhan, Mohmedyasin F. Mansuri, Peptide modelling and screening against human ace2 and spike glycoprotein rbd of sars-cov-2, In silico Pharmacol. 8 (1) (2020) 1–9.

[15] Abdul Basit, Asad Mustafa Karim, Muhammad Asif, Tanveer Ali, Jung Hun Lee, Jeong Ho Jeon, Sang Hee Lee, et al., Designing short peptides to block the interaction of sars-cov-2 and human ace2 for covid-19 therapeutics, Front. Pharmacol. (2021) 2310.

[16] Lorenzo Di Rienzo, Michele Monti, Edoardo Milanetti, Mattia Miotto, Alberto Boffi, Gian Gaetano Tartaglia, Giancarlo Ruocco, Computational optimization of angiotensin-converting enzyme 2 for sars-cov-2 spike molecular recognition, Comput. Struct. Biotechnol. J. 19 (2021) 3006–3014.

[17] Shuai Xia, Meiqin Liu, Chao Wang, Wei Xu, Qiaoshuai Lan, Siliang Feng, Feifei Qi, Linlin Bao, Lanying Du, Shuwen Liu, et al., Inhibition of sars-cov-2 (previously 2019-ncov) infection by a highly potent pan-coronavirus fusion inhibitor targeting its spike protein that harbors a high capacity to mediate membrane fusion, Cell Res. 30 (4) (2020) 343–355.

[18] Abdul Basit, Tanveer Ali, Shafiq Ur Rehman, Truncated human angiotensin converting enzyme 2; a potential inhibitor of sars-cov-2 spike glycoprotein and potent covid-19 therapeutic agent, J. Biomol. Struct. Dyn. 39 (10) (2021) 3605–3614.

[19] Mattia Miotto, Lorenzo Di Rienzo, Giorgio Gosti, Leonardo Bo', Giacomo Parisi, Roberta Piacentini, Boffi Alberto, Giancarlo Ruocco, Edoardo Milanetti, Inferring the stabilization effects of SARS-CoV-2 variants on the binding with ACE2 receptor, Commun. Biol. 5 (1) (jan 2022).

[20] Alessandro Villa, Electra Brunialti, Jessica Dellavedova, Clara Meda, Monica Rebecchi, Matteo Conti, Lorena Donnici, Raffaele De Francesco, Reggiani Angelo, Vincenzo Lionetti, et al., Dna aptamers masking angiotensin converting enzyme 2 as an innovative way to treat sars-cov-2 pandemic, Pharmacol. Res. 175 (2022), 105982.

[21] Bahaa Jawad, Puja Adhikari, Podgornik Rudolf, Ching Wai-Yim, Key interacting residues between rbd of sars-cov-2 and ace2 receptor: combination of molecular dynamics simulation and density functional calculation, J. Chem. Inf. Model. 61 (9) (2021) 4425–4441.

[22] Patrick Bryant, Gabriele Pozzati, Arne Elofsson, Improved prediction of protein-protein interactions using alphafold2, Nat. Commun. 13 (1) (2022) 1–11.

[23] Marc F. Lensink, Guillaume Brysbaert, Nurul Nadzirin, Sameer Velankar, Raphaël AG. Chaleil, Tereza Gerguri, Paul A. Bates, Elodie Laine, Alessandra Carbone, Sergei Grudinin, et al., Blind prediction of homo-and hetero-protein complexes: the casp13-capri experiment, Proteins: Struct., Funct., Bioinf. 87 (12) (2019) 1200–1221.

[24] Edoardo Milanetti, Mattia Miotto, Lorenzo Di Rienzo, Michele Monti, Giorgio Gosti, Giancarlo Ruocco, 2d zernike polynomial expansion: finding the protein-protein binding regions, Comput. Struct. Biotechnol. J. 19 (2021) 29–36.

[25] Fausta Desantis, Mattia Miotto, Lorenzo Di Rienzo, Edoardo Milanetti, Giancarlo Ruocco, Spatial organization of hydrophobic and charged residues affects protein thermal stability and binding affinity, Sci. Rep. 12 (1) (2022) 1–13.

[26] Uniprot: the universal protein knowledgebase in 2021, Nucleic Acids Res. 49 (D1) (2021) D480–D489.

[27] Szklarczyk Damian, Annika L. Gable, Katerina C. Nastou, David Lyon, Rebecca Kirsch, Sampo Pyysalo, Nadezhda T. Doncheva, Marc Legeay, Tao Fang, Bork Peer, et al., The string database in 2021: customizable protein–protein networks, and functional characterization of user-uploaded gene/measurement sets, Nucleic Acids Res. 49 (D1) (2021) D605–D612.

[28] Hong Lu, Lisa A. Cassis, Craig W. Vander Kooi, Alan Daugherty, Structure and functions of angiotensinogen, Hypertens. Res. 39 (7) (2016) 492–500.

[29] Jeffrey L. Arriza, Eliasof Scott, Michael P. Kavanaugh, Susan G. Amara, Excitatory amino acid transporter 5, a retinal glutamate transporter coupled to a chloride conductance, Proc. Natl. Acad. Sci. USA 94 (8) (1997) 4155–4160.

[30] Jared M. Lucas, Cynthia Heinlein, Tom Kim, Susana A. Hernandez, Muzdah S. Malik, Lawrence D. True, Colm Morrissey, Eva Corey, Bruce Montgomery, Elahe Mostaghel, et al., The androgen-regulated protease tmprss2 activates a proteolytic cascade involving components of the tumor microenvironment and promotes prostate cancer metastasistmprss2 influences prostate cancer metastasis, Cancer Discov. 4 (11) (2014) 1310–1325.

[31] Markus Hoffmann, Hannah Kleine-Weber, Simon Schroeder, Nadine Krüger, Tanja Herrler, Sandra Erichsen, Tobias S. Schiergens, Georg Herrler, Nai-Huei Wu, Andreas Nitsche, et al., Sars-cov-2 cell entry depends on ace2 and tmprss2 and is blocked by a clinically proven protease inhibitor, Cell 181 (2) (2020) 271–280.

[32] Ruochen Zang, Maria Florencia Gomez Castro, Broc T. McCune, Qiru Zeng, Paul W. Rothlauf, Naomi M. Sonnek, Zhuoming Liu, Kevin F. Brulois, Xin Wang, Harry B. Greenberg, et al., Tmprss2 and tmprss4 promote sars-cov-2 infection of human small intestinal enterocytes, Sci. Immunol. 5 (47) (2020), eabc3582.

[33] Michał B. Ponczek, High molecular weight kininogen: a review of the structural literature, Int. J. Mol. Sci. 22 (24) (2021), 13370.

[34] Allen P. Kaplan, Berhane Ghebrehiwet, Pathways for bradykinin formation and interrelationship with complement as a cause of edematous lung in covid-19 patients, J. Allergy Clin. Immunol. 147 (2) (2021) 507–509.
[35] Iris Schvartz, Dalia Seger, Shmuel Shaltiel, Vitronectin, Int. J. Biochem. Cell Biol. 31 (5) (1999) 539–544.
[36] Ute Reuning, Integrin $\alpha v\beta 3$ promotes vitronectin gene expression in human ovarian cancer cells by implicating rel transcription factors, J. Cell. Biochem. 112 (7) (2011) 1909–1919.
[37] Yoshikazu Takada, Xiaojing Ye, Simon Scott, The integrins, Genome Biol. 8 (5) (2007) 1–9.
[38] Ilaria Barchetta, Marco Giorgio Baroni, Olle Melander, Maria Gisella Cavallo, New insights in the control of fat homeostasis: the role of neurotensin, Int. J. Mol. Sci. 23 (4) (2022) 2209.
[39] Charles L. Bevins, Nita H. Salzman, Paneth cells, antimicrobial peptides and maintenance of intestinal homeostasis, Nat. Rev. Microbiol. 9 (5) (2011) 356–368.
[40] Heng F. Seow, Stefan Bröer, Angelika Bröer, Charles G. Bailey, Simon J. Potter, Juleen A. Cavanaugh, John EJ. Rasko, Hartnup disorder is caused by mutations in the gene encoding the neutral amino acid transporter slc6a19, Nat. Genet. 36 (9) (2004) 1003–1007.
[41] Sonja Kowalczuk, Angelika Bröer, Nadine Tietze, Jessica M. Vanslambrouck, John EJ. Rasko, Stefan Bröer, A protein complex in the brush-border membrane explains a hartnup disorder allele, Faseb. J. 22 (8) (2008) 2880–2887.
[42] Arman A. Bashirova, Teunis BH. Geijtenbeek, Gerard CF. Van Duijnhoven, Sandra J van Vliet, Jeroen BG. Eilering, Maureen P. Martin, Li Wu, Thomas D. Martin, Viebig Nicola, Percy A. Knolle, et al., A dendritic cell–specific intercellular adhesion molecule 3–grabbing nonintegrin (dc-sign)–related protein is highly expressed on human liver sinusoidal endothelial cells and promotes hiv-1 infection, J. Exp. Med. 193 (6) (2001) 671–678.
[43] Andrea Marzi, Thomas Gramberg, Graham Simmons, Peggy Moller, Andrew J. Rennekamp, Mandy Krumbiegel, Martina Geier, Jutta Eisemann, Nadine Turza, Saunier Bertrand, et al., Dc-sign and dc-signr interact with the glycoprotein of marburg virus and the s protein of severe acute respiratory syndrome coronavirus, J. Virol. 78 (21) (2004) 12090–12095.
[44] John Jumper, Richard Evans, Pritzel Alexander, Tim Green, Michael Figurnov, Olaf Ronneberger, Kathryn Tunyasuvunakool, Russ Bates, Žídek Augustin, Potapenko Anna, et al., Highly accurate protein structure prediction with alphafold, Nature 596 (7873) (2021) 583–589.
[45] Joana Pereira, Adam J. Simpkin, Marcus D. Hartmann, Daniel J. Rigden, Ronan M. Keegan, Andrei N. Lupas, High-accuracy protein structure prediction in casp14, Proteins: Struct., Funct., Bioinf. 89 (12) (2021) 1687–1699.
[46] Brian G. Pierce, Kevin Wiehe, Howook Hwang, Bong-Hyun Kim, Thom Vreven, Zhiping Weng, Zdock server: interactive docking prediction of protein–protein complexes and symmetric multimers, Bioinformatics 30 (12) (2014) 1771–1773.
[47] Zuzana Jandova, Attilio Vittorio Vargiu, Alexandre MJJ. Bonvin, Native or non-native protein–protein docking models? molecular dynamics to the rescue, J. Chem. Theor. Comput. 17 (9) (2021) 5944–5954.
[48] Heo Lim, Hasup Lee, Chaok Seok, Galaxyrefinecomplex: refinement of protein-protein complex model structures driven by interface repacking, Sci. Rep. 6 (1) (2016) 1–10.
[49] Ariel Erijman, Eran Rosenthal, Julia M. Shifman, How structure defines affinity in protein-protein interactions, PLoS One 9 (10) (2014), e110085.
[50] S. Bonella, D. Raimondo, E. Milanetti, A. Tramontano, G. Ciccotti, Mapping the hydropathy of amino acids based on their local solvation structure, J. Phys. Chem. B 118 (24) (2014) 6604–6613.
[51] Lorenzo Di Rienzo, Mattia Miotto, Bò Leonardo, Giancarlo Ruocco, Domenico Raimondo, Edoardo Milanetti, Characterizing hydropathy of amino acid side chain in a protein environment by investigating the structural changes of water molecules network, Front. Mol. Biosci. 8 (2021), 626837.
[52] Parastoo Tarighi, Samane Eftekhari, Milad Chizari, Mahsa Sabernavaei, Davod Jafari, Parastoo Mirzabeigi, A review of potential suggested drugs for coronavirus disease (covid-19) treatment, Eur. J. Pharmacol. 895 (2021), 173890.
[53] D. Van Der Spoel, E. Lindahl, B. Hess, G. Groenhof, A.E. Mark, H.J.C. Berendsen, GROMACS: fast, flexible, and free, J. Comput. Chem. 26 (16) (2005) 1701–1718.
[54] B.R. Brooks, C.L. Brooks, A.D. Mackerell, L. Nilsson, R.J. Petrella, B. Roux, Y. Won, G. Archontis, C. Bartels, S. Boresch, A. Caflisch, L. Caves, Q. Cui, A.R. Dinner, M. Feig, S. Fischer, J. Gao, M. Hodoscek, W. Im, K. Kuczera, T. Lazaridis, J. Ma, V. Ovchinnikov, E. Paci, R.W. Pastor, C.B. Post, J.Z. Pu, M. Schaefer, B. Tidor, R. M. Venable, H.L. Woodcock, X. Wu, W. Yang, D.M. York, M. Karplus, CHARMM: the biomolecular simulation program, J. Comput. Chem. 30 (10) (July 2009) 1545–1614.
[55] William L. Jorgensen, Jayaraman Chandrasekhar, Jeffry D. Madura, Roger W. Impey, Michael L. Klein, Comparison of simple potential functions for simulating liquid water, J. Chem. Phys. 79 (2) (July 1983) 926–935.
[56] G. Bussi, D. Donadio, M. Parrinello, Canonical sampling through velocity rescaling, J. Chem. Phys. 126 (1) (January 2007), 014101.
[57] M. Parrinello, A. Rahman, Crystal structure and pair potentials: a molecular-dynamics study, Phys. Rev. Lett. 45 (14) (October 1980) 1196–1199.
[58] B. Hess, H. Bekker, H.J.C. Berendsen, J.G.E.M. Fraaije, LINCS: a linear constraint solver for molecular simulations, J. Comput. Chem. 18 (12) (September 1997) 1463–1472.
[59] T.E. III Cheatham, J.L. Miller, T. Fox, T.A. Darden, P.A. Kollman, Molecular dynamics simulations on solvated biomolecular systems: the particle mesh ewald method leads to stable trajectories of DNA, RNA, and proteins, J. Am. Chem. Soc. 117 (14) (April 1995) 4193–4194.
[60] Frederic M. Richards, Areas, volumes, packing, and protein structure, Annu. Rev. Biophys. Bioeng. 6 (1) (1977) 151–176.
[61] Edoardo Milanetti, Mattia Miotto, Lorenzo Di Rienzo, Madhu Nagaraj, Michele Monti, Thaddeus W. Golbek, Giorgio Gosti, Steven J. Roeters, Tobias Weidner, Daniel E. Otzen, et al., In-silico evidence for a two receptor based strategy of sars-cov-2, Front. Mol. Biosci. (2021) 509.
[62] Vishwesh Venkatraman, Yifeng D. Yang, Sael Lee, Daisuke Kihara, Protein-protein docking using region-based 3d zernike descriptors, BMC Bioinf. 10 (1) (2009) 407.
[63] Sebastian Daberdaku, Carlo Ferrari, Exploring the potential of 3d zernike descriptors and svm for protein–protein interface prediction, BMC Bioinf. 19 (1) (2018) 35.
[64] Alfredo De Lauro, Lorenzo Di Rienzo, Mattia Miotto, Pier Paolo Olimpieri, Edoardo Milanetti, Giancarlo Ruocco, Shape complementarity optimization of antibody–antigen interfaces: the application to SARS-CoV-2 spike protein, Front. Mol. Biosci. 9 (May 2022).
[65] Edoardo Milanetti, Domenico Raimondo, Tramontano Anna, Prediction of the permeability of neutral drugs inferred from their solvation properties, Bioinformatics 32 (8) (2016) 1163–1169.